ChemPubSoc Europe

DOI: 10.1002/chem.201404498

CHEMISTRY A European Journal Full Paper

Metal–Organic Frameworks

Selective Catalytic Behavior of a Phosphine-Tagged Metal-Organic Framework Organocatalyst

Xiaoying Xu,[a, b] Stephan M. Rummelt,[a] Flavien L. Morel,[a, b] Marco Ranocchiari,*[b] and Jeroen A. van Bokhoven*[a, b]

Abstract: Steric hindrance by a metal–organic framework (MOF) is shown to influence the outcome of a catalytic reaction by controlling the orientation of its intermediates. This is demonstrated using an organocatalyst, phosphine MOF LSK-3, which is evaluated with the aid of molecular modeling and NMR spectroscopy techniques. This report is the first application of phosphine MOFs in organocatalysis and explores the potential of a framework steric hindrance to impose selectivity on a catalytic reaction. These findings expand the opportunities for control and design of the active site in the pocket of heterogeneous catalysts.

Introduction

Metal–organic frameworks (MOFs)[1–3] have been used for interesting applications in heterogeneous catalysis,[4,5] as well as in gas storage[6,7] and drug delivery,[8] owing to their chemical/structural versatility and big pores. Catalysis by MOFs is nowadays mainly focused on metal catalysis.[9] However, these materials can also be treated like organic molecules because organic functional groups can be easily introduced into the porous and crystalline structure[10–12] and modified by post-synthetic modification (PSM).[13] It is therefore quite straightforward to think of them as pseudo-organocatalysts, and some examples in the literature have already shown this.[14–18] The group of Telfer reported a strategy to introduce a non-protected proline derivative inside a non-interpenetrated IRMOF structure.[19] Duan and co-workers used a MOF as a photoactive initiator for a physisorbed organocatalyst in the asymmetric α-alkylation of aldehydes.[20]

Organocatalytic functional groups can also be immobilized in polymers or dendrimers, and on silica supports to produce recoverable and recyclable catalysts.[21] One inevitable consequence of the heterogenization of organocatalysts—and of other molecular catalysts in general—in such amorphous supports is the loss of information on the position of the atoms at the molecular level. Due to their crystallinity, MOFs provide a unique way to recycle a molecular catalyst while exploiting the pocket *around* the active site. This concept has been demonstrated in some significant publications.[22,23] For instance, Lin and co-workers reported that the cavity of a MOF can induce reversed enantioselectivity in asymmetric catalysis.[23]

Phosphines can be employed as organocatalysts for reactions of activated alkenes and alkynes.[24] Triphenylphosphine (PPh_3) analogues have been supported on polystyrene and successfully applied in the aza-Morita–Baylis–Hillman reaction.[25–28] MOFs with free phosphine groups have also been reported. A crystalline MOF containing a 4,4′,4′′-phosphinetriyltribenzoate (ptbc) linker and Zn_4O clusters, PCM-1, was reported by Humphrey and co-workers.[29] Another MOF based on the same organic linker, PCM-10, was discovered by the same group.[30] We reported the catalytic properties of a highly stable ptbc–zirconium MOF called LSK-1, which was used to coordinate single Au^I atoms onto the framework with subsequent catalytic application.[31a] More recently, our group published the synthesis of MOFs with MOF-5 and MIL-101 topologies and pendant diphenylphosphino groups.[31b] To our knowledge, no application of phosphine MOFs in organocatalysis has been reported to date. MOFs are ideal candidates to support phosphine organocatalysts because they can provide an in-depth understanding of their catalytic behavior, as shown in this contribution. Herein we demonstrate that the framework of a MOF creates steric hindrance around the active site and determines which molecules react in different phosphine-catalyzed reactions. We confirm experimentally previous repeated claims, both from our group[9] and others,[32,33] that the restricted space in a MOF cage mimics the pocket observed in the active site of enzymes.

[a] X. Xu, S. M. Rummelt, F. L. Morel, Prof. Dr. J. A. van Bokhoven
Department of Chemistry and Applied Biosciences
Laboratory of Chemical and Bioengineering
ETH Zurich, 8093 Zürich (Switzerland)
E-mail: jeroen.vanbokhoven@chem.ethz.ch

[b] X. Xu, F. L. Morel, Dr. M. Ranocchiari, Prof. Dr. J. A. van Bokhoven
Department of Synchrotron Radiation
Laboratory for Catalysis and Sustainable Chemistry
Paul Scherrer Institute, 5232 Villigen PSI (Switzerland)
E-mail: marco.ranocchiari@psi.ch
jeroen.vanbokhoven@psi.ch

Supporting information for this article is available on the WWW under http://dx.doi.org/10.1002/chem.201404498.

Results and Discussion

Synthesis and Characterization of LSK-3

Our strategy was to synthesize a phosphine MOF (P-MOF) catalyst that featured the structural and electronic properties of PPh_3, contained sufficient pore space to accommodate sterically hindered groups, and allowed the diffusion of reactants and products during catalysis (Figure 1). PPh_3 is classically employed as a ligand in homogeneous catalysis[34] and itself functions as catalyst for Lewis-base catalyzed reactions.[24] We used diphenylphosphino moieties to produce the cubic topology of IRMOF-9,[10] derived from MOF-5. The first step was to synthesize the organic linker 2-(diphenylphosphino)-[1,1′-biphenyl]-4,4′-dicarboxylic acid (**1**) via an in situ C–C coupling followed by a previously developed catalytic P–C coupling with Pd/C as catalyst (see the Supporting Information, Scheme S1).[35] We produced our P-MOF (LSK-3), by the reaction of **1**, [1,1′-biphenyl]-4,4′-dicarboxylic acid (**2**), and $Zn(NO_3)_2{\cdot}4H_2O$ in *N*,*N*-dimethylformamide (DMF) under solvothermal conditions (Figure 1 A).[35] This synthetic procedure yielded a mixed-linker MOF (MIXMOF) with a uniform distribution of functional groups within a single crystal, whose structure is represented schematically in Figures 1 B and 1 C. Deliberate dilution of phosphine groups within the framework reserves sufficient space for catalytic processes to occur (see below).

Single crystal X-ray crystallography of LSK-3 revealed a doubly interpenetrated cubic framework with $[Zn_4O]^{6+}$ inorganic units linked by biphenyl linkers (with and without P-functionalization). LSK-3 crystallizes in the tetragonal space group $P4_2/ncm$ with lattice parameters $a = 17.2209(11)$ Å and $c = 34.229(2)$ Å (see the Supporting Information, Figure S2). The distance between the two interpenetrated networks (d_{F-F}) was 12.9 Å, which is the largest among IRMOF-9 derivatives.[10,36] A large d_{F-F} is needed to accommodate the diphenylphosphino groups, which are located exclusively on the linkers oriented in the *ab* plane. This is a unique example of a MOF in which mixed linkers of the same type and size are ordered and in preferential directions of the unit cell. Surprisingly, whereas the biphenyl rings in the *c* direction were highly disordered, those in the *ab* plane were not, and the Zn-, P-, C-, and O-atom positions in the *ab* plane could be described by anisotropic displacement parameters.

ICP analysis of the material revealed a P:Zn ratio of 0.24, and ^{1}H NMR spectroscopy after digestion of LSK-3 in DCl/[D_6]DMSO, showed the ratio of linkers **2** to **1** to be 2:1. This value was used to fix the P occupation in the single crystal X-ray diffraction analysis. The P amount, calculated by combining TGA with ^{1}H NMR spectroscopy data after digestion, was 1.6 wt%. The combined characterization data confirmed the expected $[Zn_4O(\mathbf{1})(\mathbf{2})_2]$ stoichiometry of LSK-3, in agreement with previously reported IRMOF-9 and IRMOF-10 structures.[10,19,36] Nitrogen physisorption measurements carried out at 77 K of the MOF activated with supercritical CO_2 showed the type I isotherm with BET surface area $S_{BET} = 865\ m^2g^{-1}$, and micropore volume $V_p = 0.25\ cm^3g^{-1}$. The diphenylphosphino-incorporating group on LSK-3 is stable under dried and degassed conditions. The crystals exhibit good chemical stability in solvents such as $CHCl_3$, dichloromethane, benzene, DMF and diethylformamide.

Analysis of the Connelly surface of the material (Figure 1 E and Figure S6 in the Supporting Information) showed that 2D channels with rectangular and perpendicular pore openings of 6.1 Å × 8.4 Å (Channel 2 in Figure 1 D) and 6.9 Å × 8.4 Å (Channel 1 in Figure 1 D) are formed in the absence of diphenylphosphino moieties. These channels are pitted by cavities that could theoretically contain up to two diphenylphosphino moieties (depicted in blue in Figure 1 D), and are interconnected by two types of voids of 5.9 × 6.1 × 8.4 Å and 6.7 × 6.9 × 8.4 Å (depicted in yellow in Figure 1 D). Although the open space in the blue cavities is decreased in the presence of diphenylphosphino groups (Figure 1 E), it is clear that plenty of

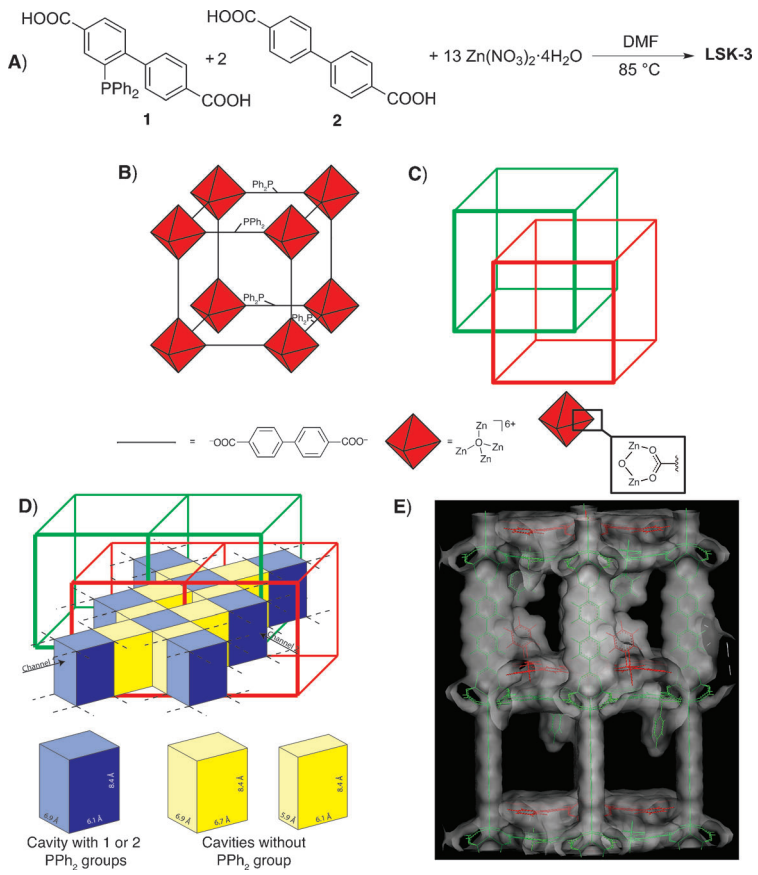

Figure 1. A) Synthesis of LSK-3. B) Schematic representation of LSK-3. Only one of the two interpenetrated frameworks is shown for clarity. For a crystal structure obtained from X-ray diffraction data, see the Supporting Information. C) Schematic structure of the two interpenetrated frameworks (each cube represents the same structure as in B). D) Schematic representation of the pore structure of LSK-3. The green and red hollow cubes are the two interpenetrated networks of the material. The blue parallelepipeds represent the cavities where one or two PPh_2 groups can be present. The yellow parallelepipeds represent the cavities without phosphine groups. E) Connelly surface of LSK-3 with two (top) or one (bottom) PPh_2 groups in one cage.

space remains for catalysis in the yellow cavities, which do not contain phosphine groups and therefore permit free diffusion of relatively large molecules. ^{31}P MAS NMR spectroscopy shows that all P atoms in LSK-3 are accessible to react with reactants (see below).

Catalytic Application of LSK-3

LSK-3 was tested as catalyst in four different types of stoichiometric and catalytic reactions with substrates of different type and size. A summary of all catalytic results is shown in Figure 2. In all reactions described below, we used samples with relatively big single crystals of size 0.5–1.0 mm (as measured by optical microscopy) to minimize the ratio between the phosphine on the surface and that inside the pores. In this way, we would indirectly prove that, if catalysis were to occur, it would do so within the pores and not just on the surface of the crystal. After all catalytic reactions, the material was recovered and analyzed either by powder X-ray diffraction (PXRD) or by polarized-light optical microscopy, which showed the single crystal integrity in all catalytic attempts below (see the Supporting Information, Figure S4). Notably, the non-functionalized IRMOF-9 failed to catalyze any of the reactions in which LSK-3 was active. We explored the synthesis of coumarin methyl 6-acetyl-2-oxo-2*H*-chromene-4-carboxylate (**3**) from 4-hydroxyacetophenone and dimethyl acetylenedicarboxylate (Figure 2A), which is a reaction requiring a stoichiometric amount of triphenylphosphine (PPh_3) in the homogeneous phase.[37] LSK-3 (100 mol% P) effected quantitative conversion to the desired coumarin **3** in $CHCl_3$ after 100 h at 80 °C. By comparison, a reaction carried out with PPh_3 at an identical phosphorus loading produced the equivalent amount of product after 120 h. Washing of the MOF with $CHCl_3$ allowed reuse of the material in a second cycle, where it mediated 89% conversion of reactants into product (Figure 2A) compared to stoichiometric reaction of PPh_3.

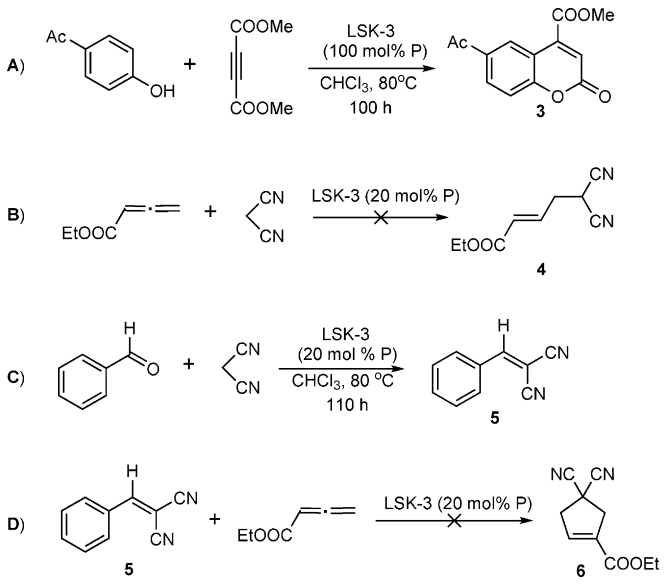

Figure 2. Reactions catalyzed by LSK-3. A) Coumarin synthesis; run 1: > 99% conversion, run 2: 89% conversion. B) Umpolung addition. C) Knoevenagel condensation; run 1: 98% conversion, run 2: 89% conversion, run 3: 73% conversion, run 4: 72% conversion. D) [3+2] cycloaddition.

Encouraged by these findings we probed the activity of LSK-3 in umpolung addition of ethyl 2,3-butanedienoate to malononitrile yielding ethyl 5,5-dicyanopent-2-enoate (**4**; Figure 2B). This reaction, when catalyzed by PPh_3 (20 mol%) in the homogeneous phase, affords the product in 73% yield.[38] LSK-3 (20 mol% P) did not produce even a trace of product under identical conditions. In an effort to further probe the impediment to this reaction we investigated the Knoevenagel condensation of benzaldehyde with malononitrile to give 2-benzylidene malononitrile (**5**; Figure 2C),[39] a reaction that is also catalyzed by amino MOFs.[40] After 110 h reaction time at 80 °C in $CHCl_3$, the conversion of benzaldehyde to product was 98%. The catalyst was recycled four times by consecutive washings with dichloromethane leading to stabilized productivity at about 70% conversion. PXRD revealed that the structure remains intact after four recycling steps. Knoevenagel condensation with our P-MOF catalyst works three times faster than the homogeneous reaction catalyzed by PPh_3, which converted only 37% of benzaldehyde after 110 h at 80 °C.

Finally, we treated the Knoevenagel product **5** with ethyl 2,3-butanedienoate and performed a [3+2] cycloaddition that we hoped would yield ethyl 4,4-dicyano-5-phenylcyclopent-1-enecarboxylate (**6**) as product (Figure 2D). Although the reaction is successfully mediated by PPh_3 catalyst (20 mol%),[41] LSK-3 (20 mol% P) did not produce any product after 60 h of reaction at 80 °C in $CHCl_3$.

Molecular Modeling and Intermediate Characterization

A number of MOF catalytic systems have shown size selectivity induced by their pore size.[42–44] However, comparison of the relative size of reactants and products (see the Supporting Information, Table S1) to the available pore opening and void space (Figure 1D,E) in LSK-3 excludes the possibility that traditional size-selectivity plays a role. In fact, the molecules participating in the umpolung reaction without any apparent conversion are actually smaller than those reacting in the successfully catalyzed coumarin synthesis. We therefore performed geometry optimization, to check the relative stability of the intermediates oriented in a different way within the MOF cage, and solid-state ^{31}P NMR spectroscopy to confirm the calculation's results. Both analyses revealed that the orientation of reaction intermediates enable or hamper reaction to occur (see below). Geometric optimizations were performed with Materials Studio from Accelrys with the Forcite molecular modeling (MM) optimization, which takes account only for steric effects and not electronic ones, followed by DMol^3 [31] DFT gradient-corrected (GGA) correlation functional of Perdew–Burke–Ernzerhof (PBE)[46] geometry optimization with the precise numerical basis set DNP 3.5 (double numerical plus polarization). Similar DFT calculations have already been successfully used in MOF geometry optimization.[47] The presence of one or two phos-

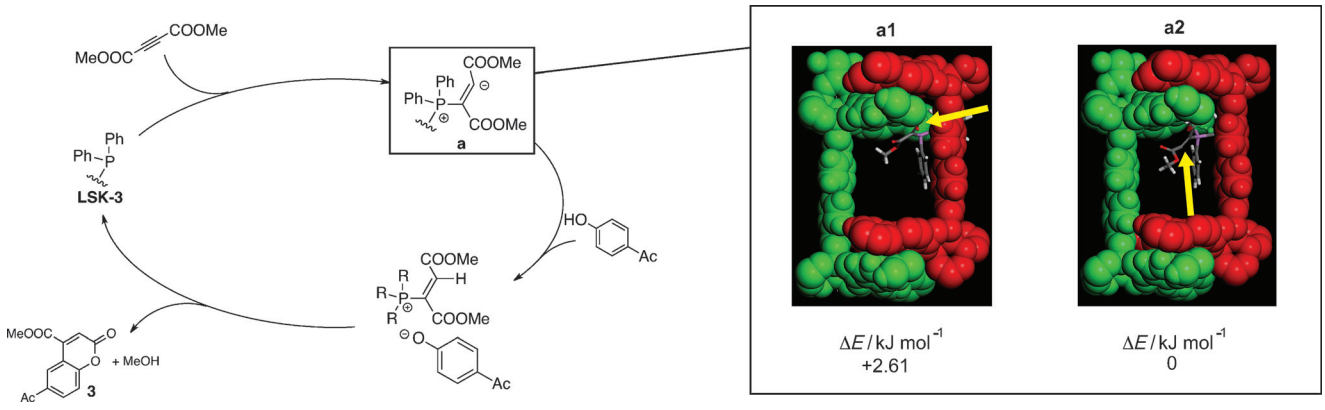

Figure 3. Mechanism and intermediates **a1** and **a2** of coumarin synthesis catalyzed by LSK-3. The yellow arrow indicates the reactive moiety of the intermediate. ΔE is the difference between the energy of the intermediates and that of the intermediate lowest in energy.

phine moieties in one cage did not change the overall outcome. We therefore restrict the discussion here to one phosphine group.

The mechanism of the phosphine-catalyzed coumarin synthesis has previously been established in the literature (Figure 3).[37] The first step involves the reaction of the phosphine with an alkyne to form a zwitterionic phosphonium salt, followed by deprotonation of phenol and formation of the phosphonium–alkene/phenolate ion couple. Subsequent aromatic substitution occurs to form the final product with cyclization, elimination of methanol, and finally regeneration of the phosphine. Geometry optimization of the zwitterionic intermediate **a** revealed two possible configurations, **a1** and **a2** (Figure 3). These are distinguished by the relative orientation of their double bonds. In the reactive intermediate **a1**, this bond is oriented towards the framework, whereas in **a2** the double bond is oriented towards the pore. We note that **a2** is slightly more stable than **a1** by 2.6 kJ mol^{-1}. ^{31}P MAS NMR and liquid-state ^{1}H NMR spectroscopy carried out under the reaction conditions confirmed the formation of the P intermediate. A stoichiometric amount of substrates and LSK-3 were loaded in a sealed glass vessel with deuterated dichloromethane and left for 1 day at 80 °C under argon atmosphere. After approximately 30% conversion of alkyne had occurred, the NMR spectrum of the solid showed no free phosphine peak at −12.6 ppm and a new peak at 30.1 ppm (see the Supporting Information, Figure S8). The latter peak is the superimposition of signals pertaining to the intermediate and the phosphine oxide adduct, which is a byproduct arising from reaction of the alkyne.[48] The quantitative disappearance of the free phosphine signal suggests that all phosphine sites are available for reaction. After completion of the reaction, the portion of the 30.1 ppm signal that relates to the adsorbed intermediate reverted to the free phosphine (peak at −12.6 ppm). The phosphine oxide contribution of the 30.1 ppm signal remained and contributed to catalyst deactivation. The analogous homogeneous reaction catalyzed by PPh_3 was also monitored by NMR spectroscopy in CD_2Cl_2. After 24 h of reactivity at 60 °C, the ^{31}P NMR spectrum showed both the intermediate at 30.7 ppm and PPh_3 at −5.0 ppm (see the Supporting Information, Figure S11).

The umpolung addition mechanism starts with the formation of the zwitterionic intermediate (**b** in Figure 4), which deprotonates malononitrile and before undergoing nucleophilic

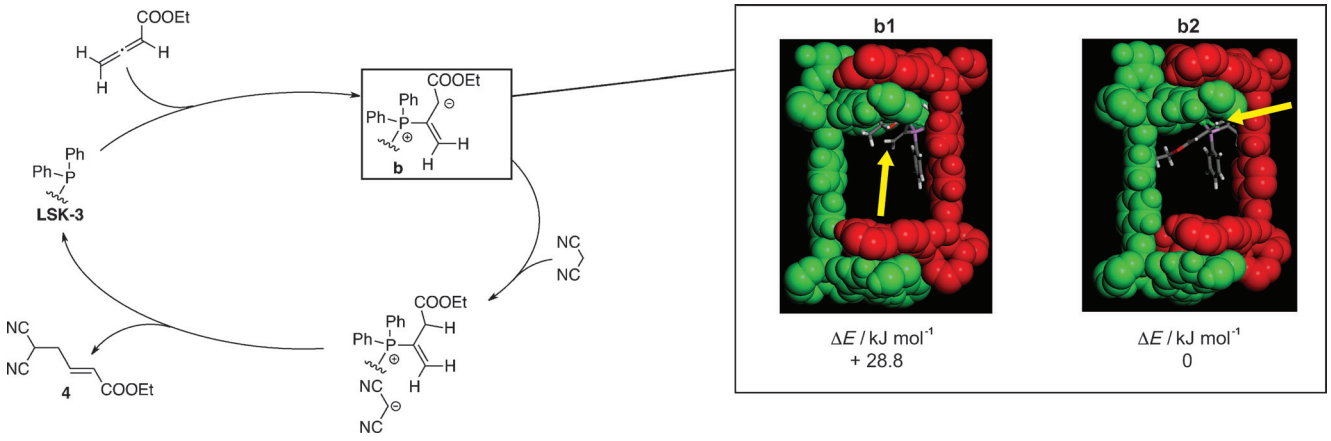

Figure 4. Mechanism and intermediates **b1** and **b2** of umpolung addition catalyzed by LSK-3. The yellow arrow indicates the reactive moiety of the intermediate.

addition. Geometry optimization of the zwitterionic intermediate **b** shows that two isomers, **b1** and **b2**, are possible. In **b1**, the double bond subject to further reaction is oriented towards the pore, whereas for **b2** this bond is oriented towards the framework. The total energy of **b2** is 28.9 kJ mol^{-1} less than that of **b1**, establishing **b2** as the favored intermediate. This disparity results from the steric hindrance by the framework, which makes the most bulky part of the intermediate, and therefore also the reactive carbon, point towards the framework. This inhibits the nucleophilic attack of deprotonated malononitrile to the protonated **b2**. This time, the energy difference is significant and explains why LSK-3 is an inactive catalyst. Solid state NMR spectroscopy confirmed our calculations, identifying an intermediate without concomitant formation of product (see the Supporting Information, Figure S9) and regeneration of free phosphine. ^{1}H NMR spectroscopic analysis of the reaction mixture indicated that no product is formed at room temperature after heating for 1 h at 60 °C (Figure S13), nor after an extended two-week period under ambient conditions. The chemical shift of the intermediate differs from that of the phosphine oxide adduct (31.2 ppm; Figure S10). In contrast, ^{1}H and ^{31}P NMR spectra of the homogeneous reaction catalyzed by PPh_3 indicated parallel formation of intermediate and product at room temperature. After heating of the liquid phase reaction for 1 h at 60 °C the signal pertaining to the intermediate disappeared with attendant reformation of free PPh_3 (Figure S12).

Modes of reactivity between substrate and the diphenylphosphino groups in LSK-3 are illustrated in Figure 5. Generally, large substituents are oriented toward the pore by the framework and consequently align reactive substituents in the same direction. When the reactive part of the intermediate is also the largest of the ancillary phosphine ligands—as is the case in our example of coumarin synthesis (Figure 5 A)—the intermediate is granted sufficient space to react with the second substrate. In contrast, steric hindrance imposed by the framework can impede further reactivity of the intermediate when the small size of a substituent induces irreversible formation of said intermediate, as for umpolung addition and [3+2] cycloaddition (Figure 5 B). In the case of the Knoevenagel condensation, the second substrate is small enough to react with a sterically restricted reactive center (Figure 5 C).

Conclusion

In summary, we have designed a novel MOF catalyst, LSK-3, which features phosphine functionalization and IRMOF-9 topology. This material demonstrated remarkable reactivity and was rationalized by a combination of molecular modeling calculations and solid-state NMR spectroscopy. We have demonstrated that it is not the size of the reactants and products that determines selectivity, but the steric hindrance by the framework, which induces a selective orientation of reaction intermediates and influences subsequent reactivity. In this way, we were able to favor certain reactions while completely inhibiting others. This is a unique feature that is observed neither in zeolites nor in previous MOF studies. The modification of the local structure inside a MOF cage represents a powerful strategy for tuning reaction selectivity to engineer the catalytic environment around the active site.

Experimental Section

Synthesis of LSK-3

[1,1′-biphenyl]-4,4′-Dicarboxylic acid (**2**; 59 mg, 0.24 mmol) and **1** (52 mg, 0.12 mmol) were placed into a 20 mL glass vial. The vial was flushed with Ar and a solution of $Zn(NO_3)_2{\cdot}4H_2O$ (286 mg, 1.51 mmol) in degassed DMF (15 mL) was added. The vial was tightly closed and kept in an oven at 85 °C for 72 h. The solvent was decanted, the crystals were washed with degassed DMF (3× 5 mL) and degassed chloroform (5 mL) was added. Chloroform was exchanged 3 times over three days and the crystals were stored in degassed toluene.

*Synthesis of coumarin **3** mediated by LSK-3*

LSK-3 (59 mg, 0.05 mmol PPh_2), 4-hydroxyacetophenone (6.8 mg, 0.05 mmol) and degassed $CHCl_3$ (1.0 mL) were placed into a dried argon-flushed 15 mL glass vial equipped with a septum. The suspension was cooled to −5 °C with an ice-salt bath, and a solution of dimethyl acetylenedicarboxylate (7.1 mg, 0.05 mmol) in de-

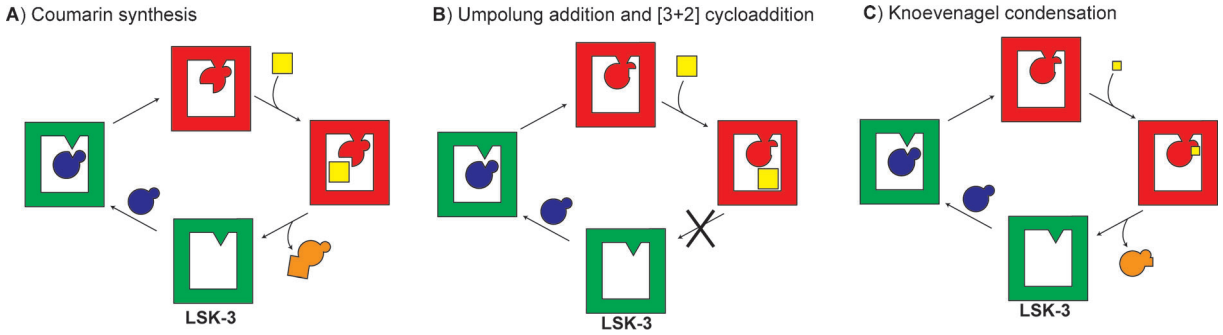

Figure 5. Schematic model that explains the reactivity of LSK-3 in the coumarin synthesis (A), umpolung and [3+2] cycloaddition (B), and Knoevenagel condensation (C). Once the first reactant (blue) approaches the active site in LSK-3 with the big substituent oriented towards the pore, it forms the intermediate (red). If the reactive part of the intermediate is oriented towards the pores (A), the intermediate can react with the second reactant (yellow) and form the product (orange). If the reactive part of the intermediate is oriented towards the framework, it reacts with the second reactant only if the latter is small enough (B, C).

gassed $CHCl_3$ (1.0 mL) was added over 20 min using a syringe. The reaction solution was warmed slowly to 80 °C and left at this temperature for 100 h. After reaction, LSK-3 was washed with degassed $CHCl_3$ (6×2 mL) within three days. $CHCl_3$ was removed from the solution by evaporation under vacuum. The final product was isolated in >99% purity by sublimation under vacuum at 140 °C. Conversion of dimethyl acetylenedicarboxylate = >99%; yield of isolated product = 95%.

Umpolung addition catalyzed by LSK-3.

LSK-3 (86 mg, 0.07 mmol PPh_2), ethyl 2,3-butadienoate (36 mg, 0.35 mmol), malononitrile (23 mg, 0.35 mmol), and degassed benzene (1.0 mL) were added into a dried argon-flushed 15 mL glass vial equipped with a septum. The vial was sealed and the reaction solution was warmed slowly to 60 °C and kept at the same temperature for 8 h. LSK-3 was washed with degassed $CHCl_3$ (6×2 mL) within three days. No product was detected by GC-MS and liquid ^{1}H NMR spectroscopy of the crude reaction mixture.

DFT calculations of the intermediates

DFT calculations with periodic boundary conditions were performed. The space group from single crystal X-ray diffraction data of LSK-3 was modified to *P*1 to allow modeling of one or two diphenylphosphino groups into the pocket. After geometry optimization using the Forcite package, the gradient corrected (GGA) correlation functional of Perdew-Burke-Ernzerhof (PBE) geometry optimization with the precise numerical basis set DNP 3.5 (double numerical plus polarization). Such calculations were carried out using the DMol^3 code as implemented in the Materials Studio package.[45]

Acknowledgements

We thank Dr. Michael Wörle for the helpful discussions and single-crystal X-ray investigation on LSK-3. We also thank the China Scholarship Council and ETH Zürich (ETHIIRA proposal ETH-33 11–1) for funding.

Keywords: heterogeneous catalysis · metal–organic frameworks · organocatalysis · phosphines · selectivity

[1] H. Li, M. Eddaoudi, M. O'Keeffe, O. M. Yaghi, *Nature* **1999**, *402*, 276–279.
[2] G. Férey, C. Mellot-Draznieks, C. Serre, F. Millange, J. Dutour, S. Surblé, I. Margiolaki, G. Ferey, S. Surble, *Science* **2005**, *309*, 2040–2042.
[3] H. Furukawa, K. E. Cordova, M. O'Keeffe, O. M. Yaghi, *Science* **2013**, *341*, 1230444.
[4] A. Corma, H. García, F. X. Llabrés i Xamena, *Chem. Rev.* **2010**, *110*, 4606–4655.
[5] J. Lee, O. K. Farha, J. Roberts, K. A. Scheidt, S. T. Nguyen, J. T. Hupp, *Chem. Soc. Rev.* **2009**, *38*, 1450–1459.
[6] E. D. Bloch, W. L. Queen, R. Krishna, J. M. Zadrozny, C. M. Brown, J. R. Long, *Science* **2012**, *335*, 1606–1610.
[7] J.-R. Li, J. Sculley, H.-C. Zhou, *Chem. Rev.* **2012**, *112*, 869–932.
[8] C.-Y. Sun, C. Qin, X.-L. Wang, Z.-M. Su, *Expert Opin. Drug Delivery* **2013**, *10*, 89–101.
[9] M. Ranocchiari, J. A. van Bokhoven, J. A. van Bokhoven, *Phys. Chem. Chem. Phys.* **2011**, *13*, 6388–6396.
[10] M. Eddaoudi, J. Kim, N. Rosi, D. Vodak, J. Wachter, M. O'Keeffe, O. M. Yaghi, *Science* **2002**, *295*, 469–472.
[11] W. Kleist, F. Jutz, M. Maciejewski, A. Baiker, *Eur. J. Inorg. Chem.* **2009**, 3552–3561.
[12] H. Deng, C. J. Doonan, H. Furukawa, R. B. Ferreira, J. Towne, C. B. Knobler, B. Wang, O. M. Yaghi, *Science* **2010**, *327*, 846–850.
[13] Z. Wang, S. M. Cohen, *Chem. Soc. Rev.* **2009**, *38*, 1315–1329.
[14] K. Tanaka, S. Oda, M. Shiro, *Chem. Commun.* **2008**, 820–822.
[15] S. Hasegawa, S. Horike, R. Matsuda, S. Furukawa, K. Mochizuki, Y. Kinoshita, S. Kitagawa, *J. Am. Chem. Soc.* **2007**, *129*, 2607–2614.
[16] Y. K. Hwang, D.-Y. Hong, J.-S. Chang, S. H. Jhung, Y.-K. Seo, J. Kim, A. Vimont, M. Daturi, C. Serre, G. Férey, *Angew. Chem. Int. Ed.* **2008**, *47*, 4144–4148; *Angew. Chem.* **2008**, *120*, 4212–4216.
[17] M. Wang, M.-H. Xie, C.-D. Wu, Y.-G. Wang, *Chem. Commun.* **2009**, 2396–2398.
[18] J. M. Roberts, B. M. Fini, A. Sarjeant, O. K. Farha, J. T. Hupp, K. Scheidt, *J. Am. Chem. Soc.* **2012**, *134*, 3334–3337.
[19] D. J. Lun, G. I. N. Waterhouse, S. G. Telfer, *J. Am. Chem. Soc.* **2011**, *133*, 5806–5809.
[20] P. Wu, C. He, J. Wang, X. Peng, X. Li, Y. An, C. Duan, *J. Am. Chem. Soc.* **2012**, *134*, 14991–14999.
[21] M. Gruttadauria, F. Giacalone, R. Noto, *Chem. Soc. Rev.* **2008**, *37*, 1666–1688.
[22] J. S. Seo, D. Whang, H. Lee, S. I. Jun, J. Oh, Y. J. Jeon, K. Kim, *Nature* **2000**, *404*, 982–986.
[23] M. Zheng, Y. Liu, C. Wang, S. Liu, W. Lin, *Chem. Sci.* **2012**, *3*, 2623.
[24] X. Lu, C. Zhang, Z. Xu, *Acc. Chem. Res.* **2001**, *34*, 535–544.
[25] D. E. Bergbreiter, C. Li, *Org. Lett.* **2003**, *5*, 2445–2447.
[26] C. K.-W. Kwong, R. Huang, M. Zhang, M. Shi, P. H. Toy, *Chem. Eur. J.* **2007**, *13*, 2369–2376.
[27] M. Fu, J. Guo, P. Toy, *Synlett* **2011**, 989–991.
[28] L. Hailing, *Prog. Chem.* **2013**, *25*, 322–329.
[29] S. M. Humphrey, P. K. Allan, S. E. Oungoulian, M. S. Ironside, E. R. Wise, *Dalton Trans.* **2009**, 2298–2305.
[30] A. J. Nuñez, L. N. Shear, N. Dahal, I. a. Ibarra, J. Yoon, Y. K. Hwang, J.-S. Chang, S. M. Humphrey, *Chem. Commun.* **2011**, 10–12.
[31] a) J. Václavík, M. Servalli, C. Lothschütz, J. Szlachetko, M. Ranocchiari, J. A. van Bokhoven, *ChemCatChem* **2013**, *5*, 692–696; b) F. L. Morel, M. Ranocchiari, J. A. van Bokhoven, *Ind. Eng. Chem. Res.* **2014**, *53*, 9120–9127.
[32] Z.-Y. Gu, J. Park, A. Raiff, Z. Wei, H.-C. Zhou, *ChemCatChem* **2014**, *6*, 67–75.
[33] M. Zhao, S. Ou, C.-D. Wu, *Acc. Chem. Res.* **2014**, *47*, 1199–1207.
[34] P. W. N. M. van Leeuwen, *Homogeneous Catalysis*, Kluwer Academic Publishers, Dordrecht, The Netherlands, **2004**.
[35] S. M. Rummelt, M. Ranocchiari, J. van Bokhoven, *Org. Lett.* **2012**, *14*, 2188–2190.
[36] M. Ranocchiari, J. A. van Bokhoven, *Chimia* **2013**, *67*, 397–402.
[37] I. Yavari, M. Adib, L. Hojabri, *Tetrahedron* **2001**, *57*, 7537–7540.
[38] C. Zhang, X. Lu, *Synlett* **1995**, 645–646.
[39] J. S. Yadav, B. V. S. Reddy, A. K. Basak, B. Visali, A. V. Narsaiah, K. Nagaiah, *Eur. J. Org. Chem.* **2004**, 546–551.
[40] A. Dhakshinamoorthy, M. Opanasenko, J. Čejka, H. Garcia, *Adv. Synth. Catal.* **2013**, *355*, 247–268.
[41] X. Lu, Z. Lu, X. Zhang, *Tetrahedron* **2006**, *62*, 457–460.
[42] C. D. Wu, A. Hu, L. Zhang, W. B. Lin, *J. Am. Chem. Soc.* **2005**, *127*, 8940–8941.
[43] F. X. Llabrés i Xamena, A. Abad, A. Corma, H. Garcia, *J. Catal.* **2007**, *250*, 294–298.
[44] S.-H. Cho, B. Ma, S. T. Nguyen, J. T. Hupp, T. E. Albrecht-Schmitt, *Chem. Commun.* **2006**, 2563–2565.
[45] B. Delley, *J. Chem. Phys.* **1990**, *92*, 508.
[46] J. Perdew, K. Burke, M. Ernzerhof, *Phys. Rev. Lett.* **1996**, *77*, 3865–3868.
[47] W. Mu, D. Liu, Q. Yang, C. Zhong, *Microporous Mesoporous Mater.* **2010**, *130*, 76–82.
[48] S. N. Arbuzova, *ARKIVOC* **2011**, 183.

Received: July 21, 2014
Published online on October 3, 2014